Density functional theory study of CO2 capture with transition metal oxides and hydroxides

Bo Zhang, Yuhua Duan, and Karl Johnson

Additional information on J. Chem. Phys.

Density functional theory study of CO$_2$ capture with transition metal oxides and hydroxides

Bo Zhang,[1,2] Yuhua Duan,[1] and Karl Johnson[1,2,a]

[1]United States Department of Energy, National Energy Technology Laboratory, Pittsburgh, Pennsylvania 15236, USA
[2]Department of Chemical and Petroleum Engineering, University of Pittsburgh, Pittsburgh, Pennsylvania 15261, USA

We have used density functional theory (DFT) employing several different exchange-correlation functionals (PW91, PBE, PBEsol, TPSS, and revTPSS) coupled with lattice dynamics calculations to compute the thermodynamics of CO$_2$ absorption/desorption reactions for selected transition metal oxides, (TMO), and hydroxides, TM(OH)$_2$, where TM = Mn, Ni, Zn, and Cd. The van't Hoff plots, which describe the reaction equilibrium as a function of the partial pressures of CO$_2$ and H$_2$O as well as temperature, were computed from DFT total energies, complemented by the free energy contribution of solids and gases from lattice dynamics and statistical mechanics, respectively. We find that the PBEsol functional calculations are generally in better agreement with experimental phase equilibrium data compared with the other functionals we tested. In contrast, the formation enthalpies of the compounds are better computed with the TPSS and revTPSS functionals. The PBEsol functional gives better equilibrium properties due to a partial cancellation of errors in the enthalpies of formation. We have identified all CO$_2$ capture reactions that lie on the Gibbs free energy convex hull as a function of temperature and the partial pressures of CO$_2$ and H$_2$O for all TMO and TM(OH)$_2$ systems studied here. © 2012 American Institute of Physics. [http://dx.doi.org/10.1063/1.3684901]

I. INTRODUCTION

The current interest in CO$_2$ capture and sequestration stems from it being one of the primary greenhouse gases and the evidence indicating that CO$_2$ plays a major role in global climate change. Annual anthropogenic CO$_2$ emissions are dominated by fossil energy use (approximate 85%).[1] Coal is responsible for about 25% of the energy production, primarily in power plants.[1] Moreover, many more coal-fired power plants are expected to be constructed over the next few decades in order to meet the increasing demand for electricity.[1] It is therefore critical to be able to capture and sequester CO$_2$ from existing and future coal-fired power plants in order to mitigate climate change. The U.S. Department of Energy has established targets for carbon capture and sequestration of removing 90% of the CO$_2$ with a concomitant increase in the cost of electricity of not more than 35% in post-combustion and oxy-combustion capture technologies and less than 10% in pre-combustion capture technology.[2] In general, there are three classes of CO$_2$ capture technologies: pre-combustion capture, post-combustion capture, and oxy-fuel combustion. The concentration of CO$_2$ in flue gas (post-combustion) is 10–15 vol. % at atmospheric pressure for a typical coal fired power plant.[2] In post-combustion capture, CO$_2$ is extracted from the flue gas by various sorbents, either physically or chemically. Chemisorption (scrubbing) with aqueous monoethanolamine (MEA) is an example of a commercially available technique that is able to capture 90%

of the CO$_2$ from flue gas.[2,3] However, this technology suffers from solvent degradation[4,5] and high energy costs[6] to regenerate the solvent. For pre-combustion, CO$_2$ is mixed with syngas, which is produced from the reaction between pure oxygen mixed with recycled flue gas or steam with fuel.[2] In this situation, the partial pressure of CO$_2$ is very high (about 20–25 bar) at relatively high temperature before coming into the turbine. Oxy-fuel combustion utilizes pure oxygen as oxidant instead of traditional air to avoid NO$_x$ and to concentrate CO$_2$ for ready capture.[2]

In addition to the commercially available MEA scrubbing technology, various solid sorbents have been developed to capture CO$_2$ at potentially lower cost. There are basically two types of solid sorbents being considered, physical adsorbents and chemical absorbents. The physical adsorbent mainly utilizes its physical adsorption ability to capture CO$_2$ at relatively low temperature. Zeolites, metal organic frameworks, and activated carbon are the most widely studied physical sorbents for CO$_2$ capture.[7–11] These materials have some attractive properties such as high specific area, low cost, low regeneration energy, etc. However, water vapor in the gas feed often has a negative impact[12,13] due to competitive adsorption between water vapor and CO$_2$. Chemical absorbents consist of metal oxides, hydroxides, carbonates, and hydrotalcites. Li$_2$O,[14,15] Rb$_2$O,[16] Cs$_2$O,[17] CaO,[18,19] MgO,[19,20] BaO,[21,22] CuO,[23] Al$_2$O$_3$,[24–26] Fe$_2$O$_3$,[26] Cr$_2$O$_3$,[27,28] NaOH,[29,30] Li$_2$ZrO$_3$,[31–33] Na$_2$ZrO$_3$,[34] Mg(OH)$_2$,[35] Na$_2$CO$_3$,[36] and K$_2$CO$_3$[37–39] are currently the most studied solid sorbents for CO$_2$ capture. However, those sorbents are still in the developmental phase and not yet commercialized on a large-scale.[2]

a)Author to whom correspondence should be addressed. Electronic mail: karlj@pitt.edu.

The general formula of hydrotalcites can be expressed as $[M_{1-x}^{2+}M_x^{3+}(OH)_2]^{x+}(A_{x/m}^{m-} \cdot nH_2O)^{x-}$, where $M^{2+} = Mg^{2+}$, Ni^{2+}, Zn^{2+}, Cu^{2+}, Mn^{2+}, etc., $M^{3+} = Al^{3+}$, Fe^{3+}, Cr^{3+}, etc., $A^{m-} = CO_3^{2-}$, SO_4^{2-}, NO_3^-, Cl^-, OH^-, etc., x is normally between 0.17 and 0.33.[40] Although these hydrotalcites have favorable specific surface area, they are not very stable at high temperature[41] due to structure evolution and generally have lower CO_2 capture capacity[35] compared with other metal compounds. On the other hand, transition metal compounds have drawn little attention either experimentally or theoretically in direct CO_2 capture. Manganese[42,43] and nickel[43,44] oxides are usually used as oxygen carriers in chemical looping combustion to generate pure CO_2 because they have high oxygen capacity and high thermal stability. Feng *et al.* studied the thermodynamics of MnO and ZnO reacting with CO_2 by using FACT-STAGE, which is a commercial thermodynamic modeling software package.[19] They also conducted thermogravimetric analysis experiments of absorption of CO_2. They concluded that MnO had a high regeneration temperature, which is desirable for fuel gas applications.

Use of computational thermodynamics modeling, as typified by the calculation of phase diagrams (CALPHAD) approach, is a powerful tool for screening possible sorbents for CO_2 capture. The drawback of this method is that thermodynamic data for all components must be available as a function of the state variables. In cases where thermodynamic data are missing it is possible to generate data from first-principles electronic structure methods to fill in missing data for use in CALPHAD calculations.[45,46] Alternately, one may also screen materials based entirely upon first-principles density functional theory (DFT) calculations, as has been demonstrated for complex hydride systems.[47,48] A similar approach has been taken by Duan and co-workers for screening CO_2 capture with groups 1 and 2 metal oxides and hydroxides.[15,49] However, the accuracy of first-principles thermodynamics calculations for these materials appears to be significantly worse (about 20 kJ/mol difference[50]) than for similar calculations on complex metal hydrides (about 10 kJ/mol difference[47]). The reason for the observed decrease in accuracy has been traced primarily to inaccuracies in the DFT predictions of the reaction enthalpies.[50] The aim of this work is to assess the accuracy of five different DFT generalized gradient functionals for the prediction of the reaction thermodynamics of various transition metal oxides and hydroxides. In the process, we also screen these materials for suitability in pre-combustion and post-combustion CO_2 capture. Finally, we will test the capture suitability of studied sorbents through a theoretically rigorous linear programming method, to identify all the CO_2 thermodynamically favorable (convex hull) capture reactions as a function of temperature and partial pressures of CO_2 and H_2O.

II. METHODOLOGY AND COMPUTATIONAL DETAILS

A. Computational details

The crystal structures of solid compounds studied in this work were selected from the inorganic crystal structure database (ICSD).[51] We have chosen to use the structure with the lowest energy, as computed from DFT at zero temperature, when more than one structure is reported for a given compound.

Many calculations in this work were performed with the Vienna *ab-initio* simulation package (VASP),[52–55] which is a periodic plane-wave DFT code. Core-electron interactions were described by projector augmented-wave (PAW) potentials.[56] We used two different generalized gradient approximation (GGA) exchange-correlation functional in our VASP calculations, particularly, PW91 of Perdew and Wang[57] and PBEsol of Perdew *et al.*[58] A plane-wave basis cutoff energy of 520 eV was used for all calculations. The k-point meshes were generated using the Monkhorst-Pack method[59] with a spacing of around 0.027 Å^{-1} between k-points along the axes of the reciprocal unit cells.[15] We performed geometry relaxation of all atomic positions, cell shape, and cell volume using a stopping criterion of energy less than 0.01 meV. The conjugate gradient algorithm was used in conjunction with the PW91 functional, whereas the quasi-Newton algorithm was with the PBEsol functional because of numerical difficulties with the conjugate gradient method. Spin polarized calculations were performed for systems containing Mn and Ni.

We also performed calculations with the grid-based projector-augmented wave (GPAW) code[60] using the following fucntionals: PBE of Perdew, Burke, and Ernzerhof,[61,62] TPSS of Tao, Perdew, Staroverov, and Scuseria,[63] and revTPSS of Perdew *et al.*[64] The latter two functionals are meta-GGA functionals, which utilize non-local kinetic energy density for the occupied Kohn-Sham orbitals to better describe the exchange-correlation energy. In contrast, the PW91, PBE, and PBEsol functionals do not include the kinetic energy density. Thus, it might be expected that the TPSS and revTPSS functionals would be more accurate than the standard GGA functionals.[63,64] For comparison purposes, we used the experimental lattice constants in our calculations. The meta-GGA calculations were performed using standard GPAW PBE pseudopotentials. The energies were converged to less than 10^{-6} eV/atom using a grid spacing of 0.15 Å. For some systems that are hard to converge with TPSS or revTPSS functionals, we have increased the threshold for the integrated value of the square of the residuals of the Kohn-Sham equations to 10^{-6}, where the default was 10^{-9}. The k-point meshes were the same as used in the VASP calculations. Spin polarized calculations were also performed for systems containing Mn and Ni. We used all five functionals to calculate the ground state energies of all the solid phase and gas phase compounds.

Phonon dispersion calculations and their contribution to the free energy were obtained using the frozen-phonon technique.[65] These calculations were done in VASP with the PW91 exchange-correlation functional. The energy cutoff is the same as listed above for our total energy calculations except the structures were relaxed until the forces were less than 0.1 meV/Å. Each symmetry-nonequivalent atom was displaced along all symmetry nonequivalent directions by 0.01–0.05 Å and forces on all atoms were calculated to construct the dynamical matrix. It is necessary to use a relatively large supercell to avoid interactions between images of the

displaced atom. We have also calculated the phonon related thermodynamic properties using the PBEsol functional at the identical conditions to those calculations with the PW91 functional via frozen-phonon in VASP for Zn system and found little difference between these two functionals. Since phonon calculations are very expensive, we will use the thermal properties calculated via the frozen-phonon approach with the PW91 functional throughout the remainder of this paper.

B. Methodology

The temperature-dependent free energy of the solids can be expressed as

$$G = U + PV - TS \approx U_{DFT} + F_{phonon}, \tag{1}$$

where U_{DFT} is the electronic total energy of the material as computed by DFT (either using the PW91, PBE, PBEsol, TPSS, or the revTPSS functional), F_{phonon} is the temperature-dependent phonon free energy contribution obtained from the frozen phonon technique through DFT calculations with the PW91 functional.

We assume that the gas phase species can be treated as ideal gas, therefore, the temperature-related free energy of gas species can be written as

$$G^0 = U + PV - TS \approx U_{DFT} + U_{ZPE} + U_{trans+rot}(T) + U_{vib}(T) + PV - TS(T), \tag{2}$$

where U_{DFT} is the electronic total energy of the material as computed using DFT (either PW91 or PBEsol functional), U_{ZPE} is the zero point energy (ZPE) of the gas. We use the statistical mechanical ideal gas expressions for the translational and internal energies of gas phase species. The translational and rotational contributions are

$$U_{trans+rot} \cong \frac{5}{2}RT \tag{3}$$

for linear molecules and nonlinear molecule we use

$$U_{trans+rot} \cong \frac{6}{2}RT. \tag{4}$$

The vibrational contributions to the energy are given by

$$U_{vib} = \sum \frac{N_a h\nu}{\exp(h\nu/T) - 1} = \sum \frac{R\Theta}{\exp(\Theta/T) - 1}. \tag{5}$$

The temperature-dependent entropy is calculated from the Shomate equation from NIST chemistry webbook,[66]

$$S = A\ln(t) + Bt + \frac{Ct^2}{2} + \frac{Dt^3}{3} - \frac{E}{2t^2} + F, \tag{6}$$

where

$$t = \frac{T}{1000}, \tag{7}$$

and A–F are system dependent constants. We use the ideal gas identity

$$PV = RT, \tag{8}$$

where V is the molar volume, in Eq. (8). Finally, we obtain the free energy expression for gas phase species for linear
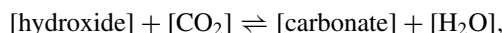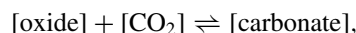
molecules as

$$G \approx U_{DFT} + U_{ZPE} + \frac{7}{2}RT$$
$$- T\left[A\ln(t) + Bt + \frac{Ct^2}{2} + \frac{Dt^3}{3} - \frac{E}{2t^2} + F\right]$$
$$+ \sum \frac{R\Theta}{\exp(\Theta/T) - 1} + RT\ln\left(\frac{P}{P_0}\right), \tag{9}$$

and for nonlinear molecules

$$G \approx U_{DFT} + U_{ZPE} + \frac{8}{2}RT$$
$$- T\left[A\ln(t) + Bt + \frac{Ct^2}{2} + \frac{Dt^3}{3} - \frac{E}{2t^2} + F\right]$$
$$+ \sum \frac{R\Theta}{\exp(\Theta/T) - 1} + RT\ln\left(\frac{P}{P_0}\right). \tag{10}$$

Combining the free energies of solid and gas species according to the following reactions:

$$[oxide] + [CO_2] \rightleftharpoons [carbonate],$$

$$[hydroxide] + [CO_2] \rightleftharpoons [carbonate] + [H_2O],$$

we can obtain the free energy change of reaction as

$$\Delta G = \Delta G_{solid} + \Delta G_{CO_2}, \tag{11}$$

or

$$\Delta G = \Delta G_{solid} + \Delta G_{CO_2} - \Delta G_{H_2O}, \tag{12}$$

where

$$\Delta G_{solid} = G_{carbonate} - G_{oxide}, \tag{13}$$

or

$$\Delta G_{solid} = G_{carbonate} - G_{hydroxide} \tag{14}$$

for reactions without and with water, respectively.

Since the volume change due to gas generation is very large relative to the volume change of solid materials, we can neglect the volume change of solid phases without significant loss of accuracy. If the activities of all solid components are taken to be 1, the equilibrium pressure of the overall reaction can then be written as

$$\frac{P_{CO_2}}{P_0} = \exp\left(-\frac{\Delta G}{RT}\right), \tag{15}$$

where P_0 is the standard state pressure (1 bar), or

$$\frac{P_{CO_2}}{P_{H_2O}} = \exp\left(-\frac{\Delta G}{RT}\right), \tag{16}$$

for reactions without and with H_2O, respectively. Note that for reactions including both CO_2 and H_2O in the gas phase, the pressure term is actually the ratio of the partial pressure of CO_2 and H_2O. The van't Hoff plots are obtained by plotting the equilibrium pressures from Eqs. (15) or (16) as a function of the inverse absolute temperature.[47]

We used a linear programming method that has been described elsewhere[48] to determine the phase diagram. In brief, the grand-canonical Gibbs free energy of a system where all

possible solid phases are in contact with a gas-phase reservoir having specified partial pressures of CO_2 and H_2O can be written as

$$G(T, \mu_{\text{gas}}) = \sum_{j=1}^{S} x^j F^j(T) - \sum_{k} \sum_{j=1}^{S} \mu_k^{\text{gas}}(T, p) x_k^{j,\text{gas}},$$

(17)

where $F^j(T)$ is the free energy of solid phase j (ignoring the pV term contribution), S is the number of solid substances, $\mu_k^{\text{gas}}(T, p)$ is the chemical potential of gas species k (CO_2 and H_2O), and x^j is the unknown mole fraction of phase j coexisting at a given composition, temperature, and pressure. The mol fraction x^j is based on elements appearing only as solids (in this case only the metals). $x_k^{j,\text{gas}}$ is the theoretical mol fraction of gas species k contained in phase j. We scanned the temperature and pressure range of interest and computed the resulting chemical potentials of each gas species, using the values in Eq. (17) to map out the convex hull. We assume ideal mixing in order to compute the thermodynamic properties of all species.

The x^j mole fractions are determined by minimizing the grand-canonical Gibbs free energy, subject to the following mass-conservation constraints for the solid phase species:

$$\sum_{i=\text{metal}}^{M} f_i = \sum_{i=\text{metal}}^{M} \sum_{j=1}^{S} x^{j,\text{solid}} b_i^{j,\text{solid}} = 1,$$

(18)

where f_i is the molar ratio of solid element i in all solids, $b_i^{j,\text{solid}}$ represents the number of atoms of type i in one formula unit of phase j, and M is the number of elements. We can choose sufficiently small intervals of temperature and pressure to ensure adequately small chemical potential changes between two steps in order to guarantee single step reactions.

III. RESULTS AND DISCUSSION

A. Lattice parameters from DFT calculations and entropies from frozen-phonon calculations

The experimental and DFT (PW91 and PBEsol functional only) optimized lattice parameters for all solids included in this study are listed in Table I, along with the enthalpies of formation and entropies from both experiments and DFT calculations. We also list experimental and calculated data for gas phase CO_2 and H_2O in Table I. Generally, good agreement can be observed between DFT calculated and experimental lattice parameters; the overall errors are within 2% for both functionals tested. We note that the predicted lattice constants from the PBEsol functional are in better agreement with experiments than predictions from PW91 for compounds containing Zn and Cd, except for $Zn(OH)_2$. The average error is less than 0.5% from PBEsol, compared with about 1.7% using PW91. However, for compounds containing Mn and Ni, the average error is 2.9% using PBESol, compared with an average error of 1.1% using PW91. The lattice parameters of hydroxides show the biggest divergence among oxides, hydroxides, and carbonates when comparing both functionals, and the average errors are 1.4% and 3.9% for PW91 and PBEsol, respectively. For compounds that have multiple re-

ported phases, the structures for the compounds listed in Table I were chosen because they have the lowest total energies from DFT calculation at 0 K. The exception is $Zn(OH)_2$, for which we have chosen the β phase, which is known to be the stable phase in experiments, although it has a slightly higher total energy than the γ phase. These structures may not be the most stable experimentally at the operating temperatures (450–600 K), and this could lead to some discrepancy between calculated and experimental thermodynamics. Identification of solid phase boundaries for multiple structures of the same compound is possible, but computationally prohibitive when the goal is to screen many different compounds.

We note from Table I that entropies calculated from the frozen-phonon approach with the PW91 functional are generally in good agreement with the experimental data. Discrepancies are within 10 J/(mol K), except for NiO, $Ni(OH)_2$, $NiCO_3$, and $MnCO_3$. This indicates our frozen-phonon approach is capable of predicting reasonable thermodynamics associated with phonons for solid materials. With all the energy and entropy terms from Eqs. (1) and (2) in hand, we can apply Eqs. (15) and (16) to construct the van't Hoff plots, as discussed in Sec. III B.

B. Thermodynamic properties for CO_2 capture reactions

Table II lists the room temperature reaction enthalpies computed from the five different DFT functionals and the entropies computed from the PW91 frozen phonon calculations for the reactions we studied. We also report data from experiments and from the HSC CHEMISTRY[67] (HSC) approach. HSC CHEMISTRY is a chemical reaction and equilibrium software package that can be used to calculate reaction equilibrium based on correlation of experimental data. The HSC CHEMISTRY package uses an equation to fit experimental heat capacity data for a very wide range of species. The resulting correlation is used along with experimental enthalpy and entropy data at 298.15 K to perform thermodynamic calculations. The HSC correlations are based on data collected from many different sources. Hence, the results from HSC CHEMISTRY calculations are not expected to agree exactly specific experimental data. We note generally good agreement between experiments and HSC in Table II. Most of the differences between experiments and HSC are less than 2 kJ/mol, although the differences are a little larger for NiO, $Ni(OH)_2$, MnO, and $Mn(OH)_2$ carbonate reactions. The largest discrepancy of about 13 kJ/mol is observed for the $Mn(OH)_2$ carbonate reaction. We conclude that the data taken from HSC are generally reliable, although discrepancies of about 10 kJ/mol may exist. On the other hand, there are relatively large differences between the calculated enthalpies of reaction at 298.15 K from all DFT methods and the experimentally measured values. The absolute mean relative errors are 49.7%, 31.8%, 16.3%, 111.5%, and 171.6% for the PW91, PBE, PBEsol, TPSS, and revTPSS functional, respectively. The PBEsol functional performs much better on average than any of the other functionals tested for the enthalpy of reaction. We also note that the enthalpies of reaction computed from lattice dynamics are only weakly dependent on temperature in the range 0 to 298 K

TABLE I. Summary of lattice parameters, enthalpies of formation, and entropies from experiments and DFT calculations with different functionals.

Compound	Space group	Lattice parameters[a]			Enthalpy of formation[b] (kJ/mol)			Entropy[c] (J/mol K)	
		Expt.	PW91	PBEsol	Expt.	PW91	PBEsol	Expt.	PW91
MnO	$Fm\bar{3}m$	a = 4.446	a = 4.3281	a = 4.3367	− 385.2	− 246.1	− 231.4	59.71	49.98
NiO	$Fm\bar{3}m$	a = 4.1944	a = 4.1809	a = 4.1056	− 239.7	− 103.7	− 108.2	37.99	53.75
ZnO	$P6_3mc$	a = 3.2525	a = 3.2806	a = 3.2389	− 350.5	− 289.7	− 288.4	43.64	45.31
		c = 5.2111	c = 5.2978	c = 5.2276					
		γ = 120	γ = 120	γ = 120					
CdO	$Fm\bar{3}m$	a = 4.6948	a = 4.7758	a = 4.7083	− 258.4	− 207.8	− 211.4	54.81	60.21
Mn(OH)$_2$	$P\bar{3}m1$	a = 3.322	a = 3.3496	a = 3.2991	− 695.4	− 529.2	− 522.7	99.2	86.15
		c = 4.734	c = 4.7417	c = 4.5419					
		γ = 120	γ = 120	γ = 120					
Ni(OH)$_2$	$P\bar{3}m1$	a = 3.13	a = 3.1665	a = 3.1203	− 529.7	− 381.9	− 397.8	88.0	70.42
		c = 4.63	c = 4.5814	c = 4.3581					
		γ = 120	γ = 120	γ = 120					
Zn(OH)$_2$	$P\bar{3}m1$	a = 3.194	a = 3.2389	a = 3.1901	− 641.9	− 540.6	− 561.3	81.2	82.59
		c = 4.714	c = 4.6598	c = 4.4824					
		γ = 120	γ = 120	γ = 120					
Cd(OH)$_2$	$I1m1$	a = 5.688	a = 5.7868	a = 5.6959	− 560.7	− 497.4	− 513.6	96.0	93.45
		b = 10.28	b = 10.2725	b = 10.0532					
		c = 3.42	c = 3.4943	c = 3.4321					
		β = 91.4	β = 88.889	β = 88.548					
MnCO$_3$	$R\bar{3}cH$	a = 4.772	a = 4.8098	a = 4.7625	− 894.1	− 699.9	− 694.0	85.8	87.71
		c = 15.637	c = 15.7615	c = 15.4107					
		γ = 120	γ = 120	γ = 120					
NiCO$_3$	$R\bar{3}cH$	a = 4.6117	a = 4.6338	a = 4.6344	− 703.4	− 532.4	− 551.2	85.4	72.99
		c = 14.735	c = 14.8239	c = 14.8197					
		γ = 120	γ = 120	γ = 120					
ZnCO$_3$	$R\bar{3}cH$	a = 4.6526	a = 4.7144	a = 4.6663	− 812.8	− 695.5	− 717.9	82.4	85.32
		c = 15.0257	c = 15.1962	c = 14.8792					
		γ = 120	γ = 120	γ = 120					
CdCO$_3$	$R\bar{3}cH$	a = 4.9207	a = 5.0071	a = 4.9614	− 750.6	− 665.5	− 678.6	92.5	100.46
		c = 16.2968	c = 16.5684	c = 16.1785					
		γ = 120	γ = 120	γ = 120					
CO$_2$	$P1$		a = 10 (fixed)		− 393.5	− 376.0	− 361.7	213.8	214.02
H$_2$O (g)	$P1$		a = 10 (fixed)		− 241.8	− 227.2	− 236.1	188.8	189.04

[a]All distances are in Å, and angles are in degrees. Experimental values are taken from ICSD database.[51]
[b]Enthalpy of formation is in kJ/mol. Experimental values are measured at 298.15 K. Most of the experimental values of solid compound are taken from Ref. 84. Experimental values for NiO and Mn(OH)$_2$ are taken from Ref. 85. Experimental values for NiCO$_3$ are taken from Ref. 86. Experimental entropies of CO$_2$ and gas H$_2$O are taken from Ref. 66. Entropies of CO$_2$ and gas H$_2$O are calculated from Shomate equation at 300 K.
[c]Entropies are in J/(mol K). Experimental values are measured at 298.15 K, entropies from frozen phonon are calculated at 300 K. Most of the experimental values of solid compound are taken from Ref. 84. Experimental values for NiO and Mn(OH)$_2$ are taken from Ref. 85. Experimental values for NiCO$_3$ are taken from Ref. 86. Experimental entropies of CO$_2$ and gas H$_2$O are taken from Ref. 66. Entropies of CO$_2$ and gas H$_2$O are calculated from Shomate equation at 300 K.

(not shown). The changes in the reaction enthalpies are less than 6 kJ/mol for oxides, and less than 2 kJ/mol for hydroxides over the temperature range from 0 to 298.15 K. This implies that one can reasonably use the zero-Kelvin DFT enthalpies for fast screening of candidate materials, which gives a substantial savings in computer time, because the phonon calculations are very computationally expensive. The entropy changes of reactions from frozen phonon calculation are generally in good agreements with experimentally measured data for every reaction studied. The differences are usually less than 10 J/(mol K), except for those reactions involving compounds containing Mn or Ni, for which the errors are above 15 J/(mol K). However, our calculated reaction entropies lie in between the HSC values listed in Table II (in the parenthesis) and the experimental data for the Mn-containing reactions, indicating that the entropies from the phonon calcula-

tions are certainly reasonable, even for these reactions. The reaction entropies for oxide carbonate reactions are all very similar, being about 170 ± 6 J/(mol K) on average, based on experimental values. In contrast, the reaction entropies for hydroxide carbonate reactions are about one order of magnitude smaller than for oxides, or about 20 ± 2 J/(mol K) on average, based on experimental values. This is partly due to the hydroxides having significantly larger entropies than the oxides, as can be seen from Table I.

The van't Hoff plots for systems containing MnO, NiO, ZnO, and CdO computed from six different methods are given in Figs. 1(a)–1(d). The first method uses PW91 DFT total energies with inclusion of finite-temperature effects, which are due to phonon contribution of solids plus the free energy of gas phase species, CO$_2$ in this case. The next four methods are identical to the first method, except that the PW91 DFT

TABLE II. Summary of reaction thermodynamics. Enthalpies are in kJ/mol, entropies in J/(mol K).

Reaction	ΔH^0 Expt.[a]	ΔH_{PW91}	ΔH_{PBE}	ΔH_{PBEsol}	ΔH_{TPSS}	$\Delta H_{revTPSS}$	ΔH HSC[c]	ΔS^0 Expt.[d]	ΔS Calc.[e]
			Calculated by DFT[b]						
$MnO + CO_2 \rightleftharpoons MnCO_3$	−115.4	−77.71	−70.27	−100.85	−95.35	−117.65	−102.77	−187.71 (−167.83)	−176.29
$NiO + CO_2 \rightleftharpoons NiCO_3$	−70.18	−52.57	−65.89	−81.27	−112.80	−141.90	−63.05	−166.39	−194.78
$ZnO + CO_2 \rightleftharpoons ZnCO_3$	−68.8	−29.63	−36.33	−67.83	−108.59	−147.30	−68.76	−175.04	−174.01
$CdO + CO_2 \rightleftharpoons CdCO_3$	−98.73	−81.50	−78.91	−105.47	−117.64	−138.89	−99.36	−176.11	−173.77
$Mn(OH)_2 + CO_2 \rightleftharpoons MnCO_3 + H_2O$	−47.0	−21.74	−16.98	−45.57	−55.70	−75.52	−33.88	−38.4 (−18.53)	−23.41
$Ni(OH)_2 + CO_2 \rightleftharpoons NiCO_3 + H_2O$	−21.98	−1.53	−22.26	−27.72	−91.57	−121.63	−14.92	−27.6	−22.40
$Zn(OH)_2 + CO_2 \rightleftharpoons ZnCO_3 + H_2O$	−19.2	−5.96	−17.88	−30.98	−90.23	−121.25	−19.18	−23.8	−22.24
$Cd(OH)_2 + CO_2 \rightleftharpoons CdCO_3 + H_2O$	−38.2	−19.11	−11.29	−39.36	−50.29	−64.39	−38.69	−28.5	−17.97

[a]All the experimental values are computed from data in Table I at 298.15 K.
[b]Enthalpies calculated with different functionals at 298.15 K including finite temperature phonon contributions.
[c]Values taken from HSC database, at 303.15 K.
[d]Experimental values are computed from data in Table I, at 298.15 K; values in the parenthesis are taken from HSC database at 303.15 K.
[e]Calculated with the PW91 functional via the frozen-phonon method at 300 K.

energies are replaced by total energies computed using the PBE, PBEsol, TPSS, and the revTPSS functionals. The last method uses the HSC package[67] to compute the van't Hoff plots. We consider the HSC calculations to be pseudo-experimental data based on agreement between experiments and HSC data reported in Table II. As can be seen from Fig. 1, the slopes from the van't Hoff plots constructed with the PW91 and PBE functional agree with those from HSC, however, the CO_2 pressure is dramatically overestimated. There is very little difference between the plots constructed by these two functionals. In contrast, the curves computed using

the TPSS and revTPSS functionals tend to underestimate the partial pressure of CO_2, with the exception of MnO, and CdO, where curves based on the TPSS functional are much closer to the HSC curves than for the other two systems. Overall, the curves computed from the PBEsol functional are in much better agreement with the HSC curves than data from the other functionals. This is especially true for ZnO, where excellent agreement can be observed.

The van't Hoff plots for reactions involving $Mn(OH)_2$, $Ni(OH)_2$, $Zn(OH)_2$, and $Cd(OH)_2$ computed from the six different methods are plotted in Fig. 2. The y axis is the ratio of
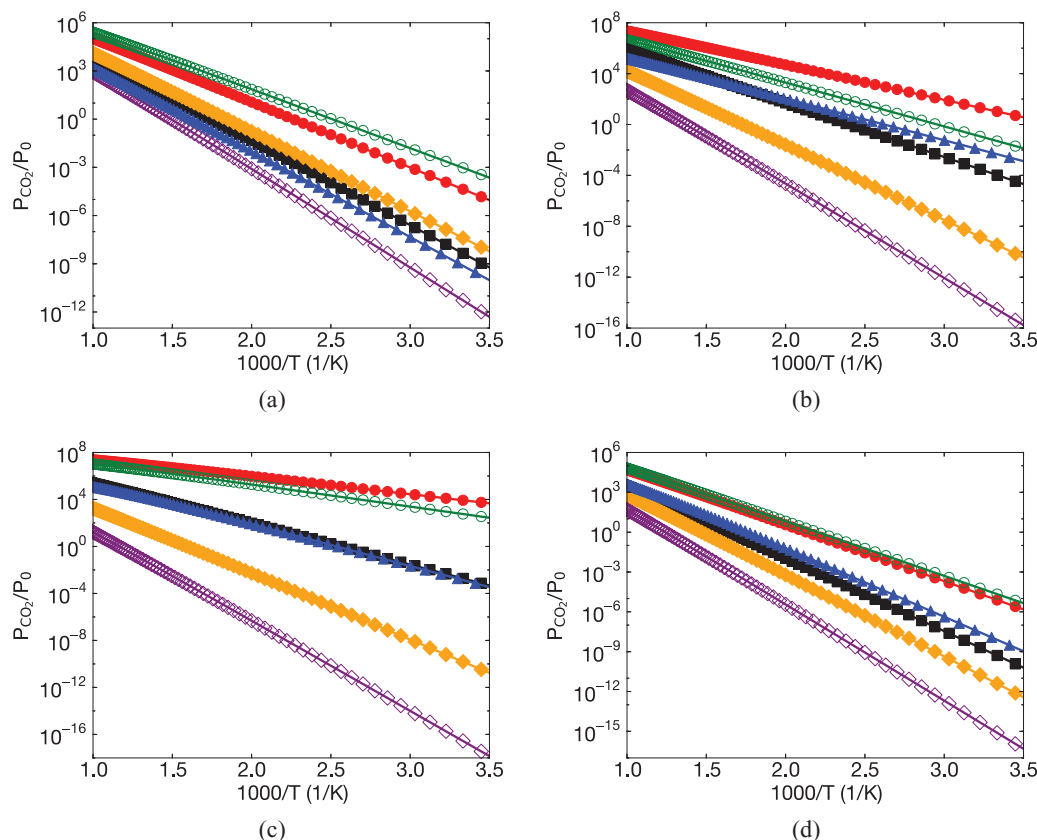

FIG. 1. The calculated van't Hoff plots for reactions of oxides with CO_2. (a) $MnO + CO_2 \rightleftharpoons MnCO_3$; (b) $NiO + CO_2 \rightleftharpoons NiCO_3$; (c) $ZnO + CO_2 \rightleftharpoons ZnCO_3$; (d) $CdO + CO_2 \rightleftharpoons CdCO_3$. The HSC data are denoted by blue triangles, PW91 by the filled red circles, PBE by the open green circles, PBEsol by the filled black squares, TPSS by the filled yellow diamonds, and revTPSS by the open purple diamonds.
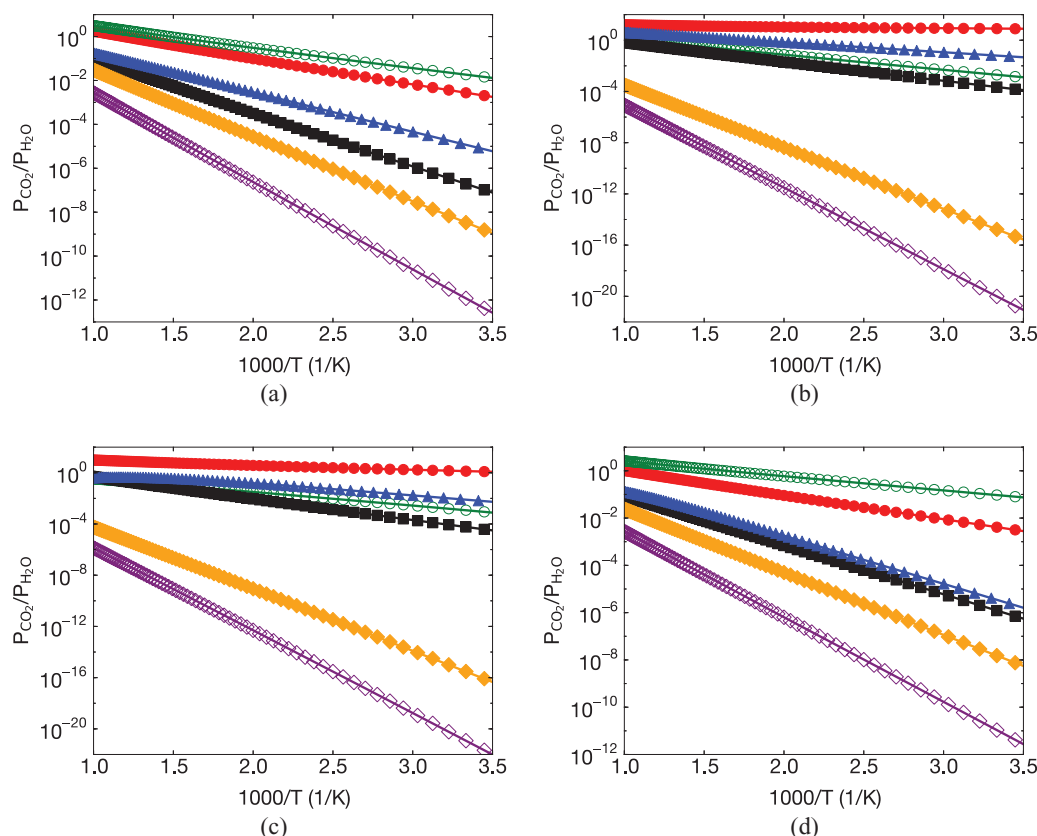
FIG. 2. The calculated van't Hoff plots for reactions of the hydroxides with CO_2. (a) $Mn(OH)_2 + CO_2 \rightleftharpoons MnCO_3 + H_2O$; (b) $Ni(OH)_2 + CO_2 \rightleftharpoons NiCO_3 + H_2O$; (c) $Zn(OH)_2 + CO_2 \rightleftharpoons ZnCO_3 + H_2O$; (d) $Cd(OH)_2 + CO_2 \rightleftharpoons CdCO_3 + H_2O$. The HSC data are denoted by blue triangles, PW91 by the filled red circles, PBE by the open green circles, PBEsol by the filled black squares, TPSS by the filled yellow diamonds, and revTPSS by the open purple diamonds.

the partial pressures of CO_2 and H_2O as given in Eq. (16). The methods used here are the same as for the oxides. The PW91 and PBE functional calculations give slopes in agreement with those from the HSC calculations, but the pressure ratios are substantially overestimated, except for $Zn(OH)_2$ where the curve using the PBE functional is closer to the HSC data than any other functionals, as is the case for the oxides. Similarly, the curves based on the energies computed from TPSS and revTPSS functionals underestimate the pressure ratio drastically. However, contrary to the oxides, the PBEsol functional significantly underestimates the pressure ratios for all systems except $Cd(OH)_2$, where good agreement between PBEsol and HSC calculations is observed.

C. Errors in computed thermodynamics

As noted previously, the reaction thermodynamics computed from DFT methods are not always in good agreement with HSC data.[50] In this section, we examine errors in the enthalpies of formation and the reaction enthalpies computed from different functionals. The differences between the formation enthalpies ($\Delta\Delta H$) from DFT and experiments for all species of interest in this work are presented in Fig. 3. It is striking that the DFT calculations result in very large errors in the formation enthalpies of the solid compounds compared with experiments, particularly for those systems containing Mn and Ni. On the other hand, the differences between calculations and experiments for gas phase species,

CO_2 and H_2O, are relatively small, but they are still too large to be considered to be within "chemical accuracy," which is about 4 kJ/mol. The mean relative errors in the formation enthalpies for gas phase H_2O and CO_2 are -5.23%, -6.20%, -5.22%, -9.57%, and -13.94% for the PW91, PBE, PBEsol, TPSS, and revTPSS functionals, respectively. All the GGA level functionals perform with comparable accuracy for the gas phase species, which are slightly better
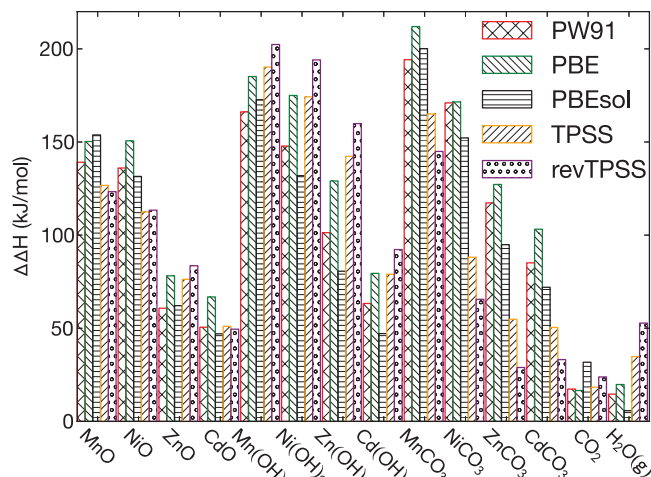

FIG. 3. Differences between the calculated and experimental enthalpies of formation, defined as $\Delta\Delta H = \Delta H_{DFT} - \Delta H_{expt}$.

TABLE III. Average percentage errors in the formation enthalpies for the systems in Fig. 3, grouped by category.

	PW91	PBE	PBEsol	TPSS	revTPSS
Oxides	− 32	− 38	− 33	− 30	− 31
Hydroxides	− 20	− 23	− 18	− 24	− 27
Carbonates	− 18	− 19	− 16	− 11	− 8
All solids	− 23	− 27	− 22	− 22	− 22
Gases	− 5	− 6	− 5	− 10	− 14

than TPSS and revTPSS functionals, but as can be seen from Fig. 3 and Table III, the errors for the solids phase species are not uniform. Notably, the relative errors for oxides are larger than those for hydroxides and carbonates. The TPSS and revTPSS functionals are better at predicting the formation enthalpies for oxides and carbonates compared with the GGA functionals, while they are slightly worse for hydroxides and the gas phase species. All the GGA functionals have similar errors in calculating the enthalpies of formation. The PBEsol functional has the smallest errors for oxides, carbonates, and gases compared with the other GGA functionals.

Given that the TPSS and revTPSS functionals give better predictions for the formation enthalpies for carbonates and oxides, one would expect that the van't Hoff plots from these two functionals to give the best agreement with the HSC data. This, however, is not the case, as can be seen from Fig. 1. In contrast, the PBEsol functional gives best agreement with the HSC van't Hoff plots among all the functionals we studied.

The reason for this is that the errors in the enthalpies of formation tend to cancel when computing the enthalpies of reaction from the PBEsol functional better than when computing the reaction enthalpies from the TPSS and revTPSS functionals. In other words, a functional that gives about the same error (of the same sign) for the oxides and the carbonates may produce reaction enthalpies for the oxide to carbonate reactions in better agreement with experimental data than a functional that gives smaller errors for the carbonates than for the oxides. This is because the heats of formation for oxides and carbonates are subtracted from one another when computing the heats of reaction.

It has been previously shown that using experimental heat of formation along with the temperature-dependent phonon contribution from DFT calculations will give better agreement with experimental and HSC data than use of the total energies from the PW91 functional.[50] We here take the same approach as a test of the PBEsol functional. We have therefore computed the van't Hoff plots using experimental formation enthalpies in place of the DFT total energies in Eqs. (1) and (2). We compare these calculations with PBEsol results and HSC data in Figs. 4(a)–4(d) for the carbonate reactions involving MnO, NiO, ZnO, and CdO. We see from Fig. 4 that the van't Hoff plots computed from PBEsol are about as accurate as those using experimental heats of formation for these oxides. The agreement between our calculated values and the HSC data is very good for Zn and Cd, not quite as good for Mn, and significantly poorer for Ni.
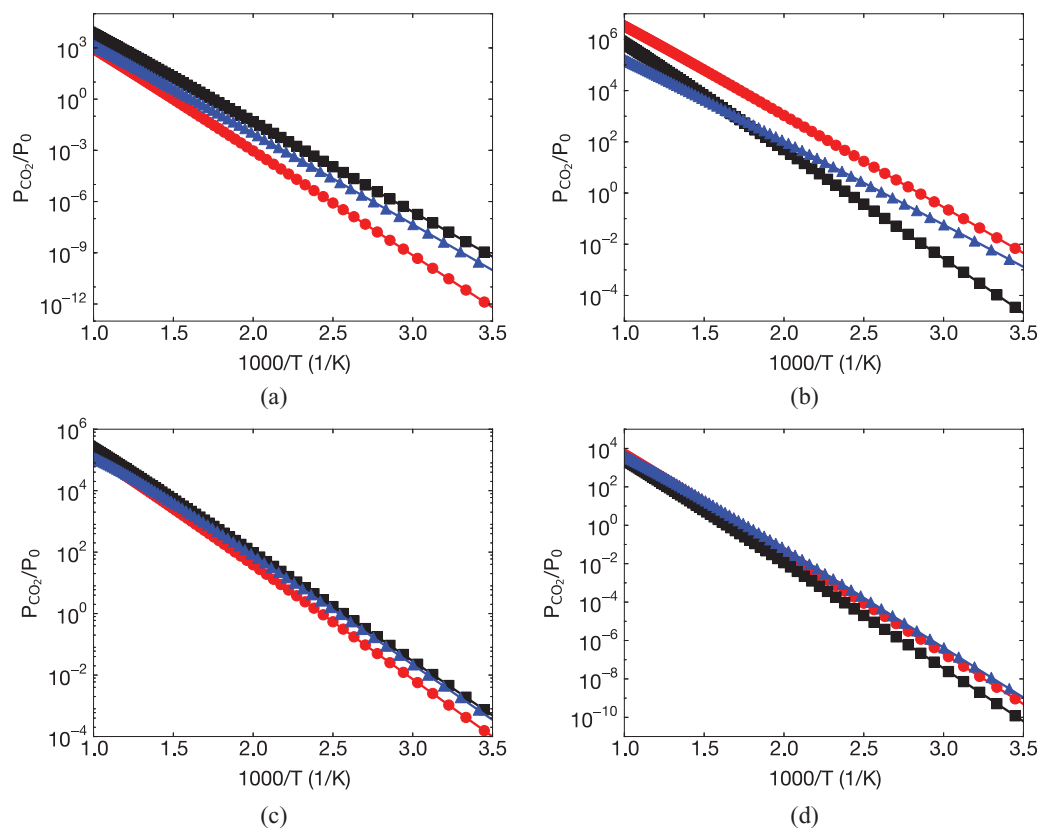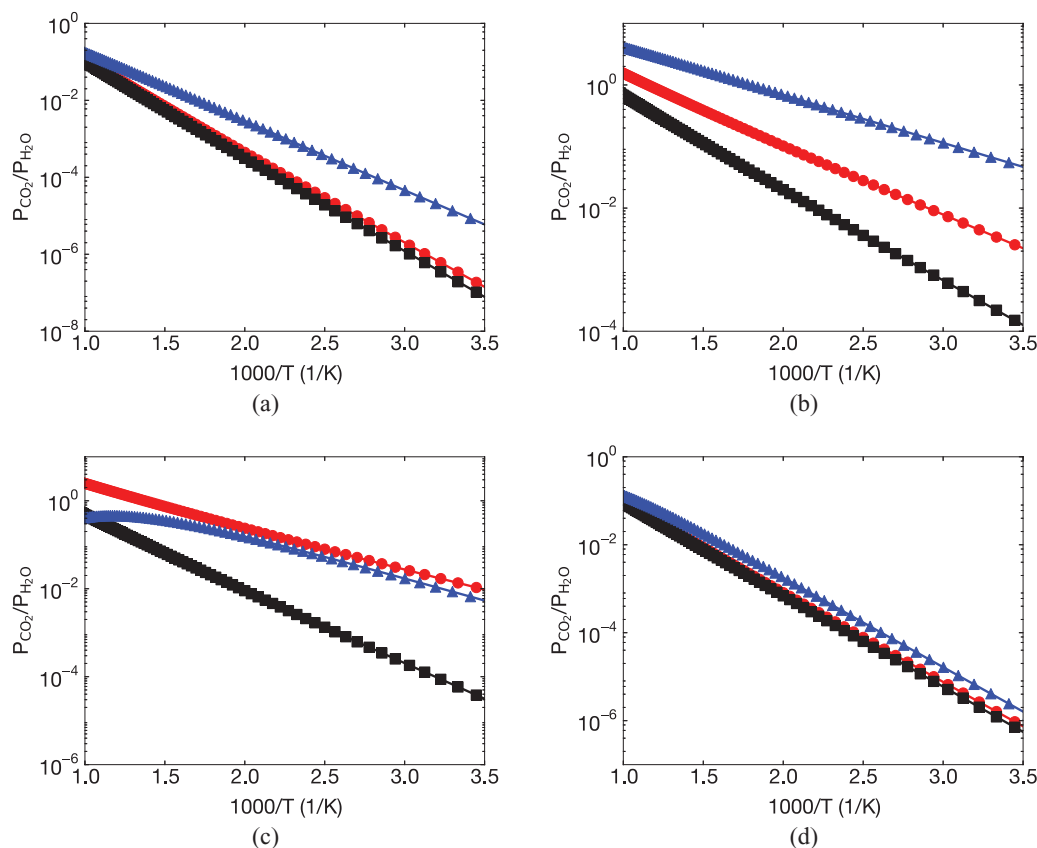

FIG. 4. Comparison of van't Hoff plots for oxides reacting with CO_2 computed from HSC data (blue triangles), from PBEsol (black squares), and from experimental heats of reaction complemented with DFT (red circles, see text for details). (a) $MnO + CO_2 \rightleftharpoons MnCO_3$; (b) $NiO + CO_2 \rightleftharpoons NiCO_3$; (c) $ZnO + CO_2 \rightleftharpoons ZnCO_3$; (d) $CdO + CO_2 \rightleftharpoons CdCO_3$.

FIG. 5. Comparison of van't Hoff plots for hydroxides reacting with CO_2 computed from HSC data (blue triangles), from PBEsol (black squares), and from experimental heats of reaction complemented with DFT (red circles, see text for details). (a) $Mn(OH)_2 + CO_2 \rightleftharpoons MnCO_3 + H_2O$; (b) $Ni(OH)_2 + CO_2 \rightleftharpoons NiCO_3 + H_2O$; (c) $Zn(OH)_2 + CO_2 \rightleftharpoons ZnCO_3 + H_2O$; (d) $Cd(OH)_2 + CO_2 \rightleftharpoons CdCO_3 + H_2O$.

The van't Hoff plots computed using the experimental formation enthalpies for the carbonate reactions involving $Mn(OH)_2$, $Ni(OH)_2$, $Zn(OH)_2$, and $Cd(OH)_2$ are plotted in Figs. 5(a)–5(d), along with plots computed from HSC data and the PBEsol functional. In general, our calculations are not in as good agreement with HSC data for the hydroxides as the oxides. For $Mn(OH)_2$ and $Cd(OH)_2$, the curves based on PBEsol energies are comparable to the curves based on experimental enthalpies of formation, but the pressure ratio of CO_2 to H_2O is significantly underestimated at low temperatures for the Mn system. For $Ni(OH)_2$ and $Zn(OH)_2$, the PBEsol calculations severely underestimate the partial pressure ratio, while the calculations using experimental heats of formation perform significantly better, although there is still a dramatic underestimation of the pressure ratio for the $Ni(OH)_2$ system.

Overall, the van't Hoff plots based on PBEsol energies have comparable accuracy to the plots computed from experimental heats of formation, except for a few cases. We therefore conclude that the PBEsol functional can be used to predict the reaction equilibrium purely from theoretical calculations with reasonable accuracy for most cases, but that one should be aware that there may be significant errors for specific systems.

We now turn to the three systems in Fig. 5 that are not in good agreement with HSC data when using the PBEsol energies, namely, reactions involving $Mn(OH)_2$, $Ni(OH)_2$, and $Zn(OH)_2$. The discrepancies between our calculations and the

HSC data can be traced back to the differences between the reaction enthalpy computed from PBEsol functional and HSC reaction enthalpies noted in Table II for these same systems. We see from Table II that the experimental reaction enthalpies for $Mn(OH)_2$ and $Ni(OH)_2$ are in poor agreement with the HSC values. This explains why use of the experimental formation energies in Figs. 5(a) and 5(b) does not result in better agreement with the HSC van't Hoff plots. It is likely that either the experimental data or the HSC data are in error for these two systems.

D. Screening materials for CO₂ capture

We have used the linear programming method to determine the phase diagrams for the TM-C-O-H systems, where TM = Mn, Ni, Zn, and Cd. All the zero-temperature energies used in the calculations were computed from the PBEsol functional and the free energy contributions for the solids were computed with the PW91 functional, as before. Figure 6 shows the calculated phase diagrams for all for TM systems at a fixed water partial pressure of 0.1 bar. These phase diagrams can be used to screen the suitability of the TM systems for CO_2 capture, based solely on thermodynamics. We note that favorable thermodynamics is a necessary but not sufficient condition for a suitable CO_2 capture material. Materials must also have acceptable kinetics for capture and regeneration, in addition to low cost, materials safety, cyclability,
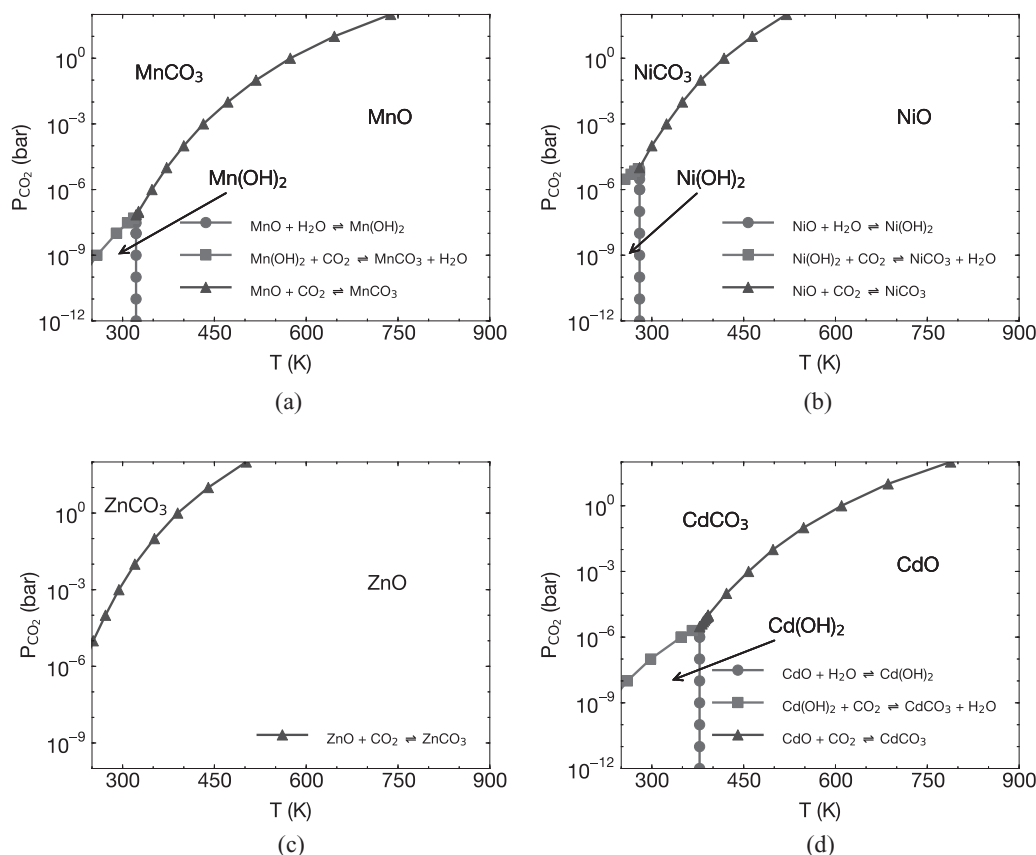
FIG. 6. Phase diagrams computed from DFT. (a) Mn–C–O–H; (b) Ni–C–O–H; (c) Zn–C–O–H; (d) Cd–C–O–H.

etc. We examine both pre- and post-combustion capture conditions and assume that capture must take place at conditions where the equilibrium pressure of CO_2 from the carbonate is at least an order of magnitude lower than partial pressure of CO_2 in the gas, and that regeneration of the material will be carried out at a temperature that would generate an equilibrium CO_2 partial pressure of about 10 bar. These are arbitrary targets, but should be a reasonable guess for practical operation. The partial CO_2 pressure for pre-combustion capture conditions is around 20–25 bar and the temperature is between 523 and 723 K to integrate with water gas shift reactor.[45] Post-combustion flue gas has a partial pressure of CO_2 of about 0.1–0.2 bar and the temperature range is from about 300 to 350 K.[48] Based on our predicted phase diagrams, we make the following observations about the suitability of the various materials for reversible CO_2 capture: The hydroxides are irrelevant for CO_2 capture for all the transition metals studied at low partial pressures of H_2O because the temperature and pressure ranges over which the hydroxide materials are stable are too low. For example, even if one started with the hydroxide phase it would likely first convert to the oxide phase before CO_2 capture, and regeneration of the carbonate phase would produce the oxide, not the hydroxide. The MnO system may be suitable for CO_2 capture under both post- and pre-combustion conditions. If we assume $P_{CO_2} = 0.1$ bar for post-combustion capture, then we see from Fig. 6 that even at the highest temperature for CO_2 capture (350 K) there is

a significant driving force for conversion of MnO to $MnCO_3$. The CO_2 could be released at about 650 K, where the partial pressure of CO_2 is about 10 bar. This is a fairly large temperature swing, which may make post-combustion capture with MnO cost prohibitive based on energy consumption. For pre-combustion, MnO will capture CO_2 at a partial pressure of about 10 bar below about 600 K and then could be regenerated by heating above 650 K to produce a stream of pure CO_2. The NiO material could be used for post-combustion capture, but not pre-combustion. Post-combustion absorption will occur below about 350 K and could be regenerated above 460 K. The equilibrium pressure of CO_2 for the NiO system at pre-combustion temperatures is too high for practical consideration. The ZnO system, like the NiO system, might be used for post- but not pre-combustion. The equilibrium temperature required to generate $P_{CO_2} = 0.1$ bar is around 350 K, while $P_{CO_2} = 10$ bar occurs at about 440 K for $ZiO/ZiCO_3$. Hence, it may be necessary to cool post-combustion gases slightly in order to have a sufficiently large driving force for ZnO to absorb CO_2; this may make this material unsuitable for post-combustion capture. Cadmium oxide could be used for both post- and pre-combustion capture, since there is a large driving force to absorb CO_2 from post-combustion flue gas; the temperature required to generate 10 bar CO_2 in this system is 680 K. Pre-combustion capture could take place at the lower end of the pre-combustion temperature range. However, the toxicity of the Cd system would preclude its wide-spread use.

E. Increasing the accuracy of DFT predictions

We have seen that DFT calculations of both reaction enthalpies and equilibrium van't Hoff plots for the systems considered here are not always in good agreement with experimental data. Ideally, one would like to be able to use DFT to predict the phase diagrams for a wide range of CO_2 capture materials with acceptable accuracy to be able to screen new materials. Our calculations indicate that this is not always the case for the functionals we have used. In this section, we discuss the possibility of using higher accuracy computational approaches to predict reaction thermodynamics. It is well known that the local-density approximation (LDA) within DFT usually underestimates lattice constants for solids, whereas GGA frequently overestimates lattice constants.[58] These trends are systematic and consistent for a large number of solids.[58] Lattice constants play an important role in determining a number of properties, for example, unit-cell geometry, volume, cohesive energy, bulk moduli, phonon frequencies, and surface energies.

The TPSS and revTPSS meta-GGA functionals are so-called "third rung" functionals in the "Jacob's ladder" approach to density functional approximations.[68] These are considered "higher level" functionals than GGA because they satisfy more fundamental constraints nonempirically.[68] The TPSS functional is based on the PBE functional while revTPSS is based on the PBEsol functional. The revTPSS functional gives improved lattice constants compared with the TPSS functional.[58,64] As noted above, the performance of the TPSS and revTPSS functionals is better than GGA level functionals at predicting the enthalpy of formation of carbonates and oxides (see Table III). Unfortunately, the reaction enthalpies and the associated van't Hoff plots computed with these meta-GGA functionals are not as accurate as data computed from the PBEsol functional. We speculate that this may be due to the use of pseudopotentials that are not tuned for meta-GGA functionals.

The next level beyond meta-GGA ("fourth rung") is the (semi-empirical) hybrid functional, which is constructed by introducing a certain amount of exact Fock exchange energy, while retaining part of the local or semi-local density functional exchange energy. These methods are computationally very demanding compared with conventional LDA or GGA functionals. B3LYP[60,69] is one of the most popular hybrid functionals used. However, B3LYP was designed for molecules, and the empirical parameters were computed from a fit to the atomization energies, ionization potentials, and proton affinities from Pople's G2 set.[69] Thus, it is not surprising that B3LYP does not perform much better at predicting lattice constants and atomization energies for metals than conventional LDA or GGA functionals, as shown in the work by Kresse *et al.*[70] The PBE0 (Refs. 71 and 72) and the associated HSE03 (Ref. 61) functionals are other "fourth rung" functionals available for calculating the properties of solids. In the HSE03 scheme, the Fock exchange term is split into a short- and a long-range part. Only the short range part of the Fock exchange is mixed with the DFT exchange, while the long range part is neglected, but compensated for by the corresponding PBE long range term. Thus, HSE03 is less compu-

tationally demanding than PBE0 or B3LYP. HSE03 and PBE0 functionals do improve the predicted lattice constants and bulk moduli of selected solids, but they do not improve the atomization energies for metals.[62,73] Better agreement with experiments for calculated heats of formation of selected solids have been reported using the HSE03 and PBE0 functionals compared with the conventional PBE functional.[62,73]

In addition to the different exchange-correlation functionals, there has been some work on accurate calculation of enthalpies of formation through post-Hartree Fock incremental methods[74,75] or Møller-Plesset second order DFT calculations.[76,77] However, these methods require enormous computational effects, with computations scaling like $O(N^5)$ where N is the number of electrons, and are not widely tested.

Since PBEsol functional just modifies two parameters of the original PBE functional,[58] the computational cost is essentially the same as the conventional PW91 or PBE functionals, but is much less than the meta-GGA and hybrid functionals. For instance, the CPU time needed for HSE03 functional, which is faster than PBE0 and B3LYP functional, is at best 2–4 times larger than PBE functional calculations on the same system.[78] Weighing the computational costs and accuracy of thermodynamic properties of reactions studied in this paper, PBEsol appears to be a reasonable compromise. However, we note that the accuracy of PBEsol is due in part to a cancellation of errors. Thus, there is certainly a need to develop more accurate and efficient methods for predicting the thermodynamic properties of solids and phase diagrams.

In addition to the higher level functionals discussed above, we note that the DFT+U method is a successful approach for treating strongly correlated systems.[79,80] However, it is not a predictive method in general. It is known that the calculated energies and other properties of a material strongly depend on the U_{eff} value used in the DFT+U calculations.[81–83] In some cases a single unique U_{eff} may not give both accurate geometries and energies.[81] Therefore DFT+U may not be appropriate for predicting reaction thermodynamics involving compounds were experimental values are not available.

IV. CONCLUSION

We have obtained the thermodynamic properties of transition metal oxides, hydroxides, and carbonates containing Mn, Ni, Zn, and Cd from first-principles DFT calculations using the PW91, PBE, PBEsol, TPSS, and revTPSS functionals and predicted the chemical equilibria for CO_2 capture reactions involving these materials. Generally speaking, the PBEsol functional performs better at predicting the reaction thermodynamics for oxide carbonate reactions compared with the other four functionals. Although the TPSS and revTPSS functionals are better at predicting the enthalpy of formation for oxides and carbonates, larger errors for other compounds leads to the observed drastic underestimation in the van't Hoff plots compared with HSC data. On the other hand, we believe that better agreement found in computing the van't Hoff plots using the PBEsol functional is due in part to a cancellation of errors. Specifically, errors in the heats of formation for oxides

that are partially offset by errors in the heats of formation of carbonates, which then cancel when computing the heats of reaction. The van't Hoff plots constructed using the PBEsol functional are comparable in accuracy to plots using experimental heats of formation when compared with HSC data, except for systems containing $Ni(OH)_2$ and $Zn(OH)_2$. Therefore, we believe that phase diagrams for carbon capture reactions can be predicted with reasonable accuracy within DFT using the PBEsol functional. We have also predicted their CO_2 capture performance through a theoretically rigorous linear programming method. Taking an adsorption temperature having a partial pressure of CO_2 that is at least an order of magnitude lower than the pressure of CO_2 in the gas stream and a regeneration temperature sufficient to generate 10 bar pressure of CO_2, we predict that all the oxides may be useful for post-combustion CO_2 capture. In contrast, only MnO and CdO are possibilities for pre-combustion capture. We predict that none of the hydroxides are suitable for CO_2 capture, since they will decompose at relatively low temperatures and partial pressures of CO_2.

ACKNOWLEDGMENTS

[1] IPCC Fourth Assessment Report (AR4), 2007.

[2] J. D. Figueroa, T. Fout, S. Plasynski, H. McIlvried, and R. D. Srivastava, Int. J. Greenhouse Gas Control **2**(1), 9 (2008).

[3] G. Astarita, G. Marrucci, and F. Gioia, Chem. Eng. Sci. **19**(2), 95 (1964).

[4] T. Supap, R. Idem, P. Tontiwachwuthikul, and C. Saiwan, Int. J. Greenhouse Gas Control **3**(2), 133 (2009).

[5] S. Chi and G. T. Rochelle, Ind. Eng. Chem. Res. **41**(17), 4178 (2002).

[6] M. R. M. Abu-Zahra, J. P. M. Niederer, P. H. M. Feron, and G. F. Versteeg, Int. J. Greenhouse Gas Control **1**(2), 135 (2007).

[7] E. Diaz, E. Munoz, A. Vega, and S. Ordonez, Ind. Eng. Chem. Res. **47**(2), 412 (2007).

[8] C. Pevida, M. G. Plaza, B. Arias, J. Fermoso, F. Rubiera, and J. J. Pis, Appl. Surf. Sci. **254**(22), 7165 (2008).

[9] J. Liu, S. Keskin, D. S. Sholl, and J. K. Johnson, J. Phys. Chem. C **115**(25), 12560 (2011).

[10] R. Banerjee, H. Furukawa, D. Britt, C. Knobler, M. O'Keeffe, and O. M. Yaghi, J. Am. Chem. Soc. **131**(11), 3875 (2009).

[11] R. Banerjee, A. Phan, B. Wang, C. Knobler, H. Furukawa, M. O'Keeffe, and O. M. Yaghi, Science **319**(5865), 939 (2008).

[12] F. Brandani and D. M. Ruthven, Ind. Eng. Chem. Res. **43**(26), 8339 (2004).

[13] Y. Wang, Y. Zhou, C. Liu, and L. Zhou, Colloids Surf., A **322**(1–3), 14 (2008).

[14] H. A. Mosqueda, C. Vazquez, P. Bosch, and H. Pfeiffer, Chem. Mater. **18**(9), 2307 (2006).

[15] Y. Duan and D. C. Sorescu, Phys. Rev. B: Condens. Matter **79**, 014301 (2009).

[16] E. J. Doskocil, S. V. Bordawekar, and R. J. Davis, J. Catal. **169**(1), 327 (1997).

[17] J. Tai, Q. Ge, R. J. Davis, and M. Neurock, J. Phys. Chem. B **108**(43), 16798 (2004).

[18] N. H. Florin and A. T. Harris, Energy Fuels **22**(4), 2734 (2008).

[19] B. Feng, H. An, and E. Tan, Energy Fuels **21**(2), 426 (2007).

[20] S. C. Lee, H. J. Chae, S. J. Lee, B. Y. Choi, C. K. Yi, J. B. Lee, C. K. Ryu, and J. C. Kim, Environ. Sci. Technol. **42**(8), 2736 (2008).

[21] K. Mudiyanselage, C. W. Yi, and J. Szanyi, Langmuir **25**(18), 10820 (2009).

[22] M. Tutuianu, O. R. Inderwildi, W. G. Bessler, and J. Warnatz, J. Phys. Chem. B **110**(35), 17484 (2006).

[23] M. Pohl and A. Otto, Surf. Sci. **406**(1–3), 125 (1998).

[24] M. Casarin, D. Falcomer, A. Glisenti, and A. Vittadini, Inorg. Chem. **42**(2), 436 (2003).

[25] M. Casarin, D. Falcomer, and A. Vittadini, Surf. Sci. **566–568**(2), 890 (2004).

[26] J. Baltrusaitis, J. H. Jensen, and V. H. Grassian, J. Phys. Chem. B **110**(24), 12005 (2006).

[27] S. Funk, T. Nurkic, B. Hokkanen, and U. Burghaus, Appl. Surf. Sci. **253**(17), 7108 (2007).

[28] O. Seiferth, K. Wolter, B. Dillmann, G. Klivenyi, H. J. Freund, D. Scarano, and A. Zecchina, Surf. Sci. **421**(1–2), 176 (1999).

[29] R. V. Siriwardane, C. Robinson, M. Shen, and T. Simonyi, Energy Fuels **21**(4), 2088 (2007).

[30] J. K. Stolaroff, D. W. Keith, and G. V. Lowry, Environ. Sci. Technol. **42**(8), 2728 (2008).

[31] E. Ochoa-Fernandez, M. Ronning, T. Grande, and D. Chen, Chem. Mater. **18**(25), 6037 (2006).

[32] E. Ochoa-Fernandez, M. Ronning, T. Grande, and D. Chen, Chem. Mater. **18**(6), 1383 (2006).

[33] Y. Duan, J. Renewable Sustainable Energy **3**(1), 013102 (2011).

[34] T. Zhao, E. Ochoa-Fernández, M. Rønning, and D. Chen, Chem. Mater. **19**(13), 3294 (2007).

[35] R. V. Siriwardane and R. W. Stevens, Jr., Ind. Eng. Chem. Res. **48**(4), 2135 (2009).

[36] Y. Liang, D. P. Harrison, R. P. Gupta, D. A. Green, and W. J. McMichael, Energy Fuels **18**(2), 569 (2004).

[37] C. Zhao and X. Chen, Energy Fuels **23**(9), 4683 (2009).

[38] S. C. Lee, B. Y. Choi, T. J. Lee, C. K. Ryu, Y. S. Ahn, and J. C. Kim, Catal. Today **111**(3–4), 385 (2006).

[39] S. C. Lee and J. C. Kim, Catal. Surv. Asia **11**(4), 171 (2007).

[40] Z. Yong and A. E. Rodrigues, Energy Convers. Manage. **43**(14), 1865 (2002).

[41] M. K. Ram Reddy, Z. P. Xu, G. Q. Lu, and J. C. Diniz da Costa, Ind. Eng. Chem. Res. **45**(22), 7504 (2006).

[42] P. Cho, T. Mattisson, and A. Lyngfelt, Fuel **83**(9), 1215 (2004).

[43] R. Siriwardane, H. Tian, G. Richards, T. Simonyi, and J. Poston, Energy Fuels **23**(8), 3885 (2009).

[44] R. Siriwardane, J. Poston, K. Chaudhari, A. Zinn, T. Simonyi, and C. Robinson, Energy Fuels **21**(3), 1582 (2007).

[45] B. P. Burton, N. Dupin, S. G. Fries, G. Grimvall, A. Fernández Guillermet, P. Miodownik, W. A. Oates, and V. Vinograd, Z. Metallkd. **92**(6), 514 (2001).

[46] C. Wolverton, X. Y. Yan, R. Vijayaraghavan, and V. Ozoliņš, Acta Mater. **50**(9), 2187 (2002).

[47] S. V. Alapati, J. K. Johnson, and D. S. Sholl, J. Phys. Chem. C **111**(4), 1584 (2007).

[48] A. R. Akbarzadeh, V. Ozoliņš, and C. Wolverton, Adv. Mater. **19**(20), 3233 (2007).

[49] Y. Duan and D. C. Sorescu, J. Chem. Phys. **133**(7), 074508 (2010).

[50] Y. Duan, B. Zhang, D. C. Sorescu, and J. K. Johnson, J. Solid State Chem. **184**(2), 304 (2011).

[51] See http://www.fiz-karlsruhe.de/icsd.html for inorganic crystal structure.

[52] G. Kresse and J. Hafner, Phys. Rev. B: Condens. Matter **47**, 558 (1993).

[53] G. Kresse and J. Hafner, Phys. Rev. B: Condens. Matter **49**, 14251 (1994).

[54] G. Kresse and J. Furthmüller, Phys. Rev. B: Condens. Matter **54**, 11169 (1996).

[55] G. Kresse and J. Furthmüller, Comput. Mater. Sci. **6**, 15 (1996).

[56] G. Kresse and D. Joubert, Phys. Rev. B: Condens. Matter **59**, 1758 (1999).

[57] J. P. Perdew, J. A. Chevary, S. H. Vosko, K. A. Jackson, M. R. Pederson, D. J. Singh, and C. Fiolhais, Phys. Rev. B: Condens. Matter **46**, 6671 (1992).

[58] J. P. Perdew, A. Ruzsinszky, G. I. Csonka, O. A. Vydrov, G. E. Scuseria, L. A. Constantin, X. Zhou, and K. Burke, Phys. Rev. Lett. **100**(13), 136406 (2008).

[59] H. J. Monkhorst and J. D. Pack, Phys. Rev. B: Condens. Matter **13**, 5188 (1976).

[60] P. J. Stephens, F. J. Devlin, C. F. Chabalowski, and M. J. Frisch, J. Phys. Chem. **98**(45), 11623 (1994).

[61] J. Heyd, G. E. Scuseria, and M. Ernzerhof, J. Chem. Phys. **118**(18), 8207 (2003).

[62] J. Paier, M. Marsman, K. Hummer, G. Kresse, I. C. Gerber, and J. G. Angyan, J. Chem. Phys. **124**(15), 154709 (2006).

[63] J. Tao, J. P. Perdew, V. N. Staroverov, and G. E. Scuseria, Phys. Rev. Lett. **91**(14), 146401 (2003).

[64] J. P. Perdew, A. Ruzsinszky, G. I. Csonka, L. A. Constantin, and J. Sun, Phys. Rev. Lett. **103**(2), 026403 (2009).

[65]G. J. Ackland, J. Phys. Condens. Matter **14**, 2975 (2002).

[66]M. W. J. Chase, *NIST-JANAF Thermochemical Tables*, 4th ed. (American Institute of Physics, Melville, NY, 1998).

[67]HSC CHEMISTRY Software, version 6.1 (Outotec Research).

[68]Z. K. Liu, J. Phase Equilib. Diffus. **30**(5), 517 (2009).

[69]A. D. Becke, J. Chem. Phys. **98**(7), 5648 (1993).

[70]J. Paier, M. Marsman, and G. Kresse, J. Chem. Phys. **127**(2), 024103 (2007).

[71]M. Ernzerhof and G. E. Scuseria, J. Chem. Phys. **110**(11), 5029 (1999).

[72]C. Adamo and V. Barone, J. Chem. Phys. **110**(13), 6158 (1999).

[73]M. Marsman, J. Paier, A. Stroppa, and G. Kresse, J. Phys. Condens. Matter **20**(6), 064201 (2008).

[74]K. Doll, M. Dolg, P. Fulde, and H. Stoll, Phys. Rev. B: Condens. Matter **55**(16), 10282 (1997).

[75]F. R. Manby, D. Alfè, and M. J. Gillan, Phys. Chem. Chem. Phys. **8**(44), 5178 (2006).

[76]S. Casassa, M. Halo, L. Maschio, C. Roetti, and C. Pisani, Theor. Chem. Acc. **117**(5-6), 781 (2007).

[77]M. Marsman, A. Grüneis, J. Paier, and G. Kresse, J. Chem. Phys. **130**(18), 184103 (2009).

[78]J. Heyd and G. E. Scuseria, J. Chem. Phys. **121**(3), 1187 (2004).

[79]V. I. Anisimov, F. Aryasetiawan, and A. I. Lichtenstein, J. Phys. Condens. Matter **9**(4), 767 (1997).

[80]V. I. Anisimov, J. Zaanen, and O. K. Andersen, Phys. Rev. B: Condens. Matter **44**(3), 943 (1991).

[81]J. L. F. Da Silva, M. V. Ganduglia-Pirovano, J. Sauer, V. Bayer, and G. Kresse, Phys. Rev. B: Condens. Matter **75**(4), 045121 (2007).

[82]A. Jain, G. Hautier, S. P. Ong, C. J. Moore, C. C. Fischer, K. A. Persson, and G. Ceder, Phys. Rev. B: Condens. Matter **84**(4), 045115 (2011).

[83]S. Lutfalla, V. Shapovalov, and A. T. Bell, J. Chem. Theory Comput. **7**(7), 2218 (2011).

[84]D. R. Lide, *CRC Handbook of Chemistry and Physics*, 84th ed. (CRC, Boca Raton, FL, 2003).

[85]J. A. Dean, *Lange's Handbook of Chemistry*, 15th ed. (McGraw-Hill, New York, 1998).

[86]D. G. Archer, J. Phys. Chem. Ref. Data **28**, 1485 (1999).